JOC The Journal of Organic Chemistry

Article

pubs.acs.org/joc

# Quantum-Mechanical Study of the Reaction Mechanism for 2π−2π Cycloaddition of Fluorinated Methylene Groups

Andrew R. Motz,[†] Andrew M. Herring,[†] Shubham Vyas,*[,‡] and C. Mark Maupin*[,†]

[†]Department of Chemical & Biological Engineering, Colorado School of Mines, Golden, Colorado 80401, United States

[‡]Department of Chemistry, Colorado School of Mines, Golden, Colorado 80401, United States

Supporting Information

**ABSTRACT:** Perfluorocyclobutyl polymers are thermally and chemically stable, may be produced without a catalyst via thermal 2π−2π cycloaddition, and can form block structures, making them suitable for commercialization of specialty polymers. Thermal 2π−2π cycloaddition is a rare reaction that begins in the singlet state and proceeds through a triplet intermediate to form an energetically stable four-membered ring in the singlet state. This reaction involves two changes in spin state and, thus, two spin-crossover transitions. Presented here are density functional theory calculations that evaluate the energetics and reaction mechanisms for the dimerizations of two different polyfluorinated precursors, 1,1,2-trifluoro-2-(trifluoromethoxy)ethane and hexafluoropropylene. The spin-crossover transition states are thoroughly investigated, revealing important kinetics steps and an activation energy for the gas-phase cycloaddition of two hexafluoropropene molecules of 36.9 kcal/mol, which is in good agreement with the experimentally determined value of 34.3 kcal/mol. It is found that the first carbon−carbon bond formation is the rate-limiting step, followed by a rotation about the newly formed bond in the triplet state that results in the formation of the second carbon−carbon bond. Targeting the rotation of the C−C bond, a set of parameters were obtained that best produce high molecular weight polymers using this chemistry.

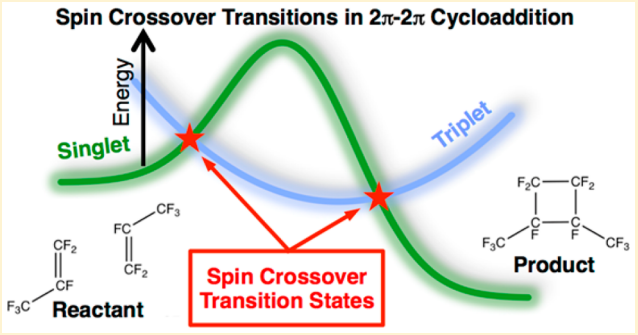


## 1. INTRODUCTION

During Teflon's development at E.I. Du Pont de Nemours and Company, Lewis and Naylor[1] discovered an unexpected product after a pyrolysis experiment, octafluorocyclobutane. They proposed a reaction mechanism where two tetrafluoroethylene molecules would react via 2π−2π, thermally induced cycloaddition. Bartlett et al. later showed that a similar reaction between 1,1-dichloro-2,2-difluoroethylene and dienes had a preferred direction, namely, the difluoromethylene group bonds with the terminal carbons of the diene, and using stereochemistry arguments concluded it passed through a diradical intermediate.[2,3] It has also been shown that trifluorovinyl ethers are able to undergo this cycloaddition.[4,5] Using electron paramagnetic resonance (EPR), the predicted diradical triplet intermediate has been observed experimentally for the cycloaddition of 4,4′-bis(4-trifluorovinyloxy)biphenyl (TFVE-BP).[6] In order for this diradical triplet intermediate to exist, the reaction mechanism must involve at least two changes of spin (i.e., singlet to triplet and back to a singlet), as the reactants and product are both in the singlet state. This study proposes a full reaction mechanism using density functional calculations to find spin-crossover transition states (SCO-TSs) for the dimerization of 1,1,2-trifluoro-2-(trifluoromethoxy)ethene (TFVE) and the dimerization of hexafluoropropylene (HFP). This unique chemistry has practical applications in polymerization reactions where molecules with two TFVE functional groups are able to form linear polymers containing perfluorocyclobutyl groups. The versatility of the functional group on these polymers has been previously demonstrated, highlighting their potentially broad properties[7] and thus broad range of applications from waveguides,[8] fuel cell electrolytes,[9,10] to coatings for space applications.[11]

These polymers are produced without a catalyst or small molecule evolving, making perfluorocyclobutyl polymers suitable for production of specialty plastics on a commercial scale. Additionally, because this reaction only involves a rearrangement of bonds, TFVE polymers are able to reversibly repair damage caused from mechanical strain via heating.[12] These properties make them ideal for a diverse array of specialty chemical applications. A complete understanding of this reaction mechanism is vital for rational design of polymerization conditions ranging from benchtop to commercial scale.

Computational chemistry is able to give insight into entire reaction pathways, thus providing details on geometry and molecular motions that are not accessible through experiments alone. The cycloaddition of fluorinated vinyl groups involves

Received: March 13, 2017
Published: May 26, 2017





DOI: 10.1021/acs.joc.7b00597
J. Org. Chem. 2017, 82, 6578−6585

formation of a diradical triplet intermediate, which requires passage through two SCO-TSs. A SCO-TS is defined as a local minimum on the seam of intersection between the potential energy surfaces of different spin states. Harvey[13] gives an in-depth review on reactions involving SCO-TS steps and establishes a methodology for studying such reactions. Each energy surface exists as a 3N-dimensional surface; therefore, the crossing of surfaces is a 3N-1-dimensional hypersurface. In order to find the seam of intersection, two constraints must be met: (1) the energy of the two spin states are equal and (2) the geometry of the two spin states are the same. While any point on the seam of intersection is a possible point of crossing from one spin state to another, the minimum on this seam represents a point on the minimum energy path for spin state crossing. SCO-TSs are not saddle points on a single energy surface but rather a saddle point on an adiabatic surface defined by two different spin-state surfaces. Therefore, traditional methods of finding transition states are not applicable, and a modified method must be utilized.

## 2. METHODS

To evaluate the $2\pi-2\pi$ cycloaddition of fluorinated methylene groups, two different model cyclodimerization reactions were studied. The first reaction consisted of the cyclodimerization of two HFP molecules, and the second reaction was the cyclodimerization of two TFVE molecules (Figure 1).

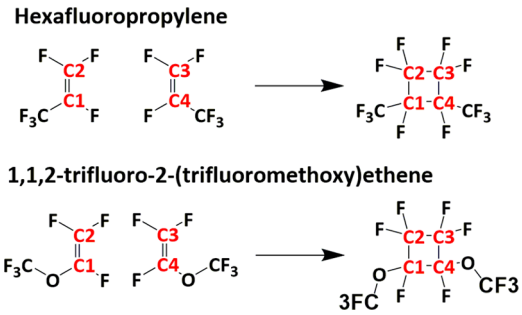


**Figure 1.** Overall cycloaddition reaction for (top) HFP and (bottom) TFVE. The $\pi$ bonds rearrange, forming new $\sigma$ bonds. Note that both *cis* and *trans* conformations of the $-OCF_3$ and $-CF_3$ substituents in the final product are possible, and the above figure is intended to be the general reaction.

All geometry optimizations were performed using the UM06-2X density functional and the 6-311G(d,p) basis set as implemented in the Gaussian09 software package.[14−16] The main product of this reaction is the 1,2 adduct where the ethers are on adjacent carbons, while a minor amount of the 1,3 adduct has been detected via $^{19}F$ NMR.[17] This same study indicates that the 1,2 adduct was composed of nearly equal amounts of *cis* and *trans* products. Additionally, it has been experimentally determined that the rate of *cis* to *trans* rotation occurs at a rate which is 10× faster than that of the ring-closure reaction.[2,3] To limit the scope of this study, only the *cis* conformation of the substituents was considered, as seen in Figure 2. In accordance with traditional nomenclature, C2 and C3 will be referred to as head carbons and C1 and C4 will be referred to as tail carbons. Looking at Figure 2, one can observe that head-to-head and tail-to-tail reactions will form the main product, while head-to-tail reactions will form the 1,3 adduct, a side product. All three reaction mechanisms are considered in this study for both TFVE and HFP.

The bond to be formed first (C1−C3, C1−C4, or C2−C3) was scanned with a singlet multiplicity from 5 to 1.4 Å in increments of 0.2 Å, starting with a dihedral of 0° between the four carbons. The geometry at 1.4 Å was then used to scan the same bond in reverse with

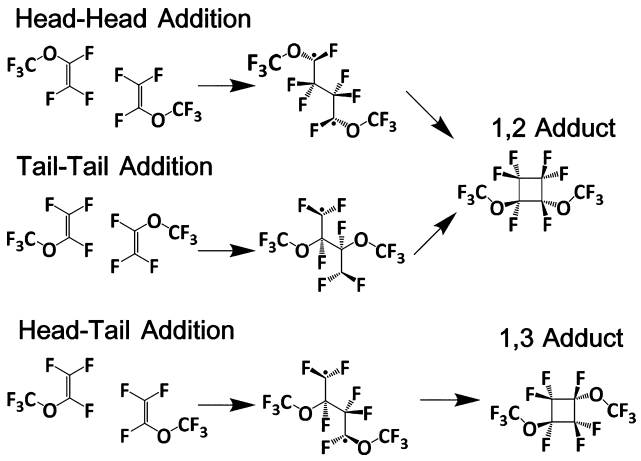


**Figure 2.** Three distinct ways for the two bonds to form in the cycloaddition of two TFVE molecules, resulting in two unique products.

a triplet multiplicity. When the two molecules approached, the relevant dihedrals (different for all three pathways) all converged to ca. 180°. For all three cases (Figure 2), the singlet energy increased when the distance between adjacent carbons (i.e., C1−C3 and C2−C4, or C1−C4 and C2−C3) was decreased, while for the triplet state the energy decreased. In the region where the energies for the singlet and triplet crossed, two-dimensional scans of the dihedral and bond length were performed. The bonds were scanned in increments of 0.05 Å over a range ±0.1 Å from the crossing point, while the dihedral was scanned in increments of 20° over a range of ±40° from the crossing point. During these calculations, only two parameters were fixed to be equivalent between the different spin state calculations, resulting in some discrepancies between the other geometric parameters.

The geometry located at the minimum on the line of intersection from the partial optimization of the singlet state was then used as the starting point for a Newton−Raphson minimization algorithm, developed in house, based on previous work from Chachiyo and Rodriguez.[18]

The unconstrained minimization of a function, $\overline{f}(\overline{x})$, can be calculated through an iterative process using eq 1 where $\overline{x}$ is a vector of variables, $A_{jk}$ is defined by eq 2, and $\Delta\overline{x}$ is the change in variables that are expected to minimize $\overline{f}(\overline{x})$. Once the change in variables is enacted, the process is iterated until a sufficient minimization threshold is achieved.

$$\Delta\overline{x}^{u} = -A^{T}(\overline{x})\overline{f}(\overline{x}) \tag{1}$$

$$A_{jk} = \frac{\partial^2 f_a}{\partial x_j \partial x_k} \tag{2}$$

Using Lagrange multipliers, a constraint, $c$, can be added, resulting in eq 3 (derived elsewhere[19]), where $B_{aj}$ is defined by eq 4.

$$\begin{aligned}\Delta\overline{x}^{c} &= \Delta\overline{x}^{u} - A^{-1}B^{T}(BA^{-1}B^{T})^{-1}(c + B\Delta\overline{x}^{u})\Delta\overline{x}^{c} \\ &= \Delta\overline{x}^{u} - A^{-1}B^{T}(BA^{-1}B^{T})^{-1}(c + B\Delta\overline{x}^{u})\end{aligned} \tag{3}$$

$$B_{aj} = \frac{\partial c_a}{\partial x_j} \tag{4}$$

By knowing $\overline{F}(\overline{x})$, $c(\overline{x})$, and their derivatives with respect to $\overline{x}$, the iterative process can take place. The function $\overline{F}(\overline{x})$ is to be minimized while meeting the constraint, $c(\overline{x})$. For finding a SCO-TS, eq 5 is minimized with the constraint that the singlet and triplet energies are equal (eq 6). The constraint restricts the solution to the seam of intersection, and then the minimum on that seam is found (here represented by the minimum of the square of the sum of energies).

$$f(\overline{x}) = (E^{S=1}(\overline{x}) + E^{S=3}(\overline{x}))^2 \tag{5}$$



DOI: 10.1021/acs.joc.7b00597
J. Org. Chem. 2017, 82, 6578−6585

$$c(\bar{x}) = 0 = E^{S=1}(\bar{x}) - E^{S=3}(\bar{x}) \quad (6)$$

A frequency calculation at both the singlet and triplet states (i.e., $s = 1$ and $s = 3$) on the resulting structures provides the required information for the calculation including the energy, gradient, and Hessian. The proposed algorithm works by first submitting a frequency calculation for both singlet and triplet states with the exact same geometries. Once the calculation is finished, the energy, gradient, and Hessian are extracted from the formatted checkpoint file. These data are then used to calculate the subsequent change in coordinates that is expected to minimize the sum of the energy, with the constraint that the energies must be equal. The coordinates are then modified, new calculations are performed, and the process is iterated until the convergence threshold is reached. This study found that taking the full calculated step size ($\Delta\bar{x}$) would tend to overshoot the roots; therefore, the step size is reduced in magnitude from 0.01 to 0.5 $\Delta\bar{x}$. This process was done for all possible SCO-TSs.

Once the SCO-TSs were identified, the products and intermediates were found through standard energy optimization procedures. Next, the SCO-TSs were analyzed using vibrational analysis developed by Glowacki, and the MESMER program was used, in conjunction with Landau−Zener theory, to account for crossing probability and to create a kinetic model.[20−24] The model was then used to predict reaction rate over a wide temperature range (200−800 K) at 1 atm. These values are reported and discussed in the next section. This data is then compared to experimentally determined reaction rates.

## 3. RESULTS AND DISCUSSION

In the literature there are many different experimental examples of fluorinated vinyl cycloadditions with a wide variety of substituents, reaction conditions, and available characterization.[25] Two model compounds, TFVE and HFP, were chosen to represent a majority of the available reactions while giving insight into how the reaction proceeds and how substituent substitution impacts the reaction. TFVE was chosen because many of the studies on cycloadditions use ether linkages to connect a trifluorovinyl group to a functional spacer group. HFP was chosen because it provides a close comparison to TFVE, without the ether linkage, and there is reliable kinetic data for that exact molecule (something that is lacking for TFVE). First, TFVE was studied, and then the substituent was altered (from $-OCF_3$ to $-CF_3$), and part of the calculations were run again with the new molecule. Three different reaction pathways were analyzed for each dimerization, representing the three different ways the two new carbon−carbon bonds can form, as discussed in section 2 and depicted in Figure 2.

**3.1. TFVE Search for Transition State.** As a preliminary search for the first transition state in each reaction pathway, a 1D scan of the carbon−carbon bond distance was conducted on the two carbon atoms participating in the bond formation. This resulted in an increased energy as the two monomers approached each other in the singlet state from 5.0 to 1.4 Å. In the triplet state, the energy decreased as the molecules approached each other, eventually reaching a minimum and then increasing in energy again upon further reduction in the separation distance. The two different energy scans are found to cross at ca. 1.8−1.9 Å as depicted in Figure 3. It was observed that the dihedral for the scans rotated to ca. 180° as the C1 and C3 distance decreased, indicating a local minimum with respect to the dihedral.

Near the intersection of the singlet and triplet 1D scans, 2D scans were performed with the additional fixed parameter being the dihedral about the newly forming C1−C3 bond. The dihedral was chosen because it was identified as a major differentiating parameter between the singlet and triplet spin states. Scanning over these two parameters (i.e., C1−C3 distance and C2−C1−C3-C4 dihedral) enables the creation of a 2D surface depicting the crossing of the singlet and triplet spin states, which are required to have the same energy and geometries. This process was repeated for both head−head and tail−tail addition reactions. The 2D data for all three seams of intersection can be seen in Figure 4.

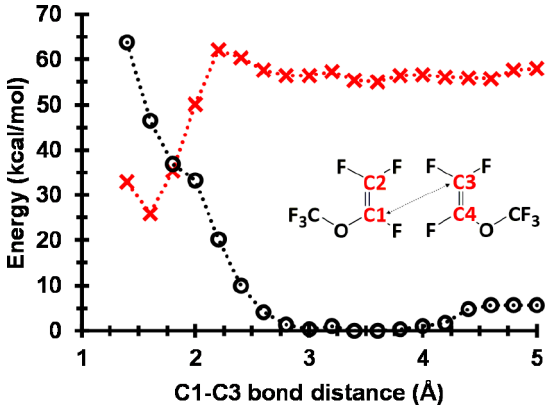


**Figure 3.** Singlet (O) and triplet (X) energy from the 1D scan of C1−C3 bond for the head to tail addition of two TFVE molecules.

The head-to-head addition was found to be the lowest energy at the crossing seam. Additional increases in steric hindrance near the reaction site resulted in an energy increase, effectively shifting the energy surfaces up. Head-to-head addition has no $-OCF_3$ near the reaction site, head-to-tail has one, and tail-to-tail has two such groups. It is important to note that the two energy surfaces have only two parameters that are fixed, and the remaining variables are allowed to freely optimize and therefore may not be identical for the two spin surfaces, which means that the minima found in the 2D scans are not the real SCO-TSs. The minima on the seams were used as the starting points for the Newton−Raphson algorithm discussed in section 2. The second SCO-TSs were found in a similar way. First, a 1D scan of dihedral was conducted, followed by a 2D scan of dihedral and bond length.

**3.2. SCO-TSs of TFVE and Full Reaction Mechanism.** The singlet geometries obtained from the minimum on the seam from the 2D scans were the starting point for the Newton−Raphson algorithm, as outlined in the Methods section. Initially the energy difference was ca. 20 kcal/mol but converged to <0.01 kcal/mol for all 6 SCO-TSs, a table with the stationary point energies along with all atomic coordinates for SCO-TSs is available in the Supporting Information. The dynamics of a well-behaved minimization is shown in Figure 5. The energy is different from that obtained from the minimum on the seam of a 2D scan, confirming that 2D scans are insufficient in determining SCO-TSs.

Once the convergence was completed for all 6 SCO-TSs, the overall reaction pathway and energy profile were constructed; see Figure 6. Note that the first SCO-TS is the rate-limiting step for all of the reaction pathways. Additionally, the activation energy increases with steric hindrance, following the observations from the 2D scan. The lowest energy pathway, head-to-head addition, forms the 1,2 adduct (P1), and the second lowest energy path forms the unique 1,3 adduct (P2). This is in alignment with experiments showing that the 1,2 adduct is the major product and the 1,3 adduct is a minor product.[17,26] Calculating the percentage of the total reaction accounted for


DOI: 10.1021/acs.joc.7b00597
J. Org. Chem. 2017, 82, 6578−6585

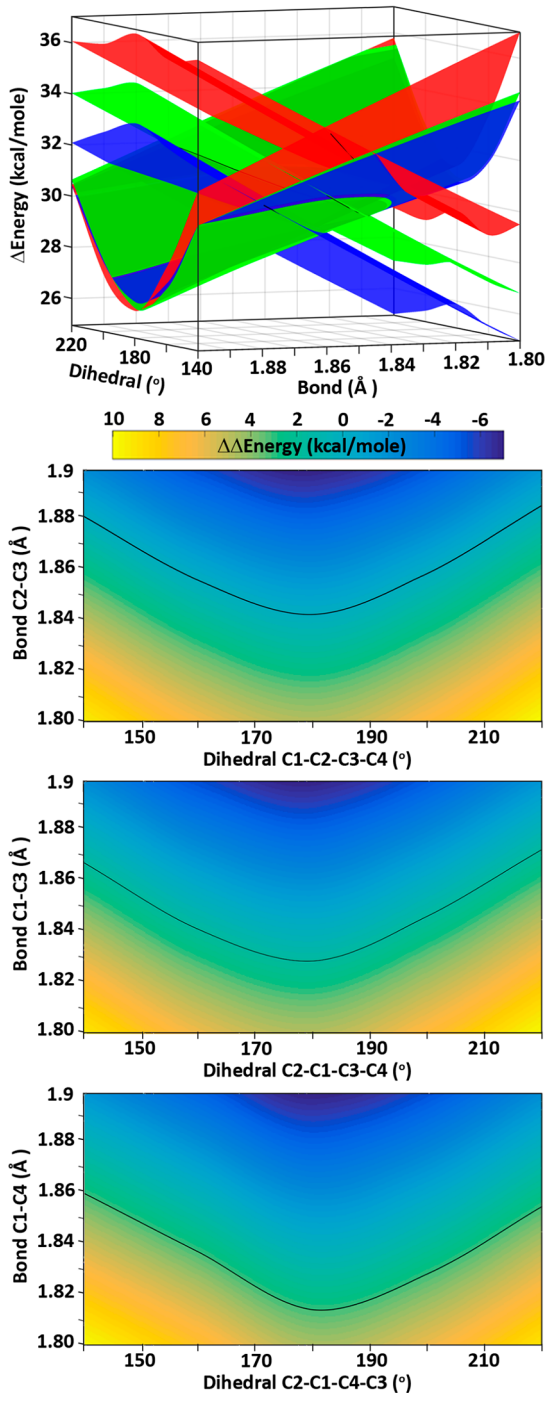


**Figure 4.** (Top) 2D scans near the seam of intersection for all three reaction methods yielded surfaces that crossed at a seam of intersection. All three seams had minima within the scanning surface. (Bottom three graphs) Isosurfaces showing the energy difference between $S = 1$ and $S = 3$ states; the steric hindrance increases down the page as an additional $-OCF_3$ group is introduced near the reaction site (head−head, head−tail, tail−tail). The surfaces are color coordinated for head−head (blue), head−tail (green), and tail−tail (red) with the singlet plane increasing in energy as the bond length decreases.

by each of the three pathways reveals that ca. 95% of the product is produced via head-to-head addition (Figure SI-1).

Looking at how the geometry evolves through the mechanisms elucidates two distinct processes (Figure 6 and Table 1). First, from the reactant to the first SCO-TS (TS1, TS3, and TS5) and to the intermediate (I1, I2, and I3) the C−C bond is forming, and thus, the distance is decreasing. After the intermediate, the bond length is almost unchanged. The second process is a twisting motion where the dihedral rotates about 180° from the first SCO-TS to the product. This coincides with EPR spectroscopy showing an axially symmetric triplet, and the diradical molecule is present in the cycloaddition reaction.[6] In the gas phase with small molecules, this twisting motion does not appear to play a significant role in the reaction rate; however, this motion is hypothesized to have significant implications in condensed phase polymerizations. This may result in a higher effective activation energy.

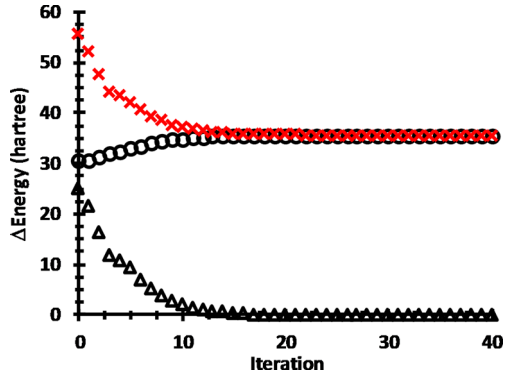


**Figure 5.** Energy convergence starting from the minimum on line of intersection from 2D scans for the singlet (O), triplet (X), and (Δ) difference between singlet and triplet energies.

**3.3. Full Mechanism of HFP.** Using the results from TFVE, the substituent was changed from $-OCF_3$ to $-CF_3$, and the Newton−Raphson minimization was conducted for all six SCO-TSs. This resulted in guesses that were close enough to produce converged structures. The reaction pathways and energy diagram for the possible HFP dimerization reactions can be found in Figure 7.

The same trends as discussed for TFVE hold true for the dimerization of HFP. The energy of the first transition state still increases with increasing steric hindrance, and the rotation about the first bond formed is still prevalent. In general, there is a higher activation energy for HFP than TFVE. Experiments correlating the fluorinated vinyl cycloaddition rate to the electronegativity of the substituent have previously predicted such behavior.[27]

The geometric parameters for all of the converged stationary points in the HFP reaction can be seen in Table 2. Once again, there are two main events of the reactions. First, there is a shortening of the C−C bond, followed by a rotation of the dihedral, as seen in Figure 7.

**3.4. Kinetic Simulations.** Because this reaction pathway contains nontraditional transition states, typical transition-state theory and kinetics needs to be modified. One method to take into account the probability of crossing from one state to another is to use the Landau−Zener formula. This was accomplished in this study through running GlowFreq and MESMER, two programs written and distributed by Glowacki.[22−24] MESMER was run at atmospheric pressure and a temperature range of 100−700 K to give a broad range of rates for each reaction. The kinetic simulation was implemented for TFVE and HFP, and the theoretical results and experimental results for HFP cycloaddition, previously reported by Atkinson,[28] are depicted in Figure 8.



DOI: 10.1021/acs.joc.7b00597
J. Org. Chem. 2017, 82, 6578−6585

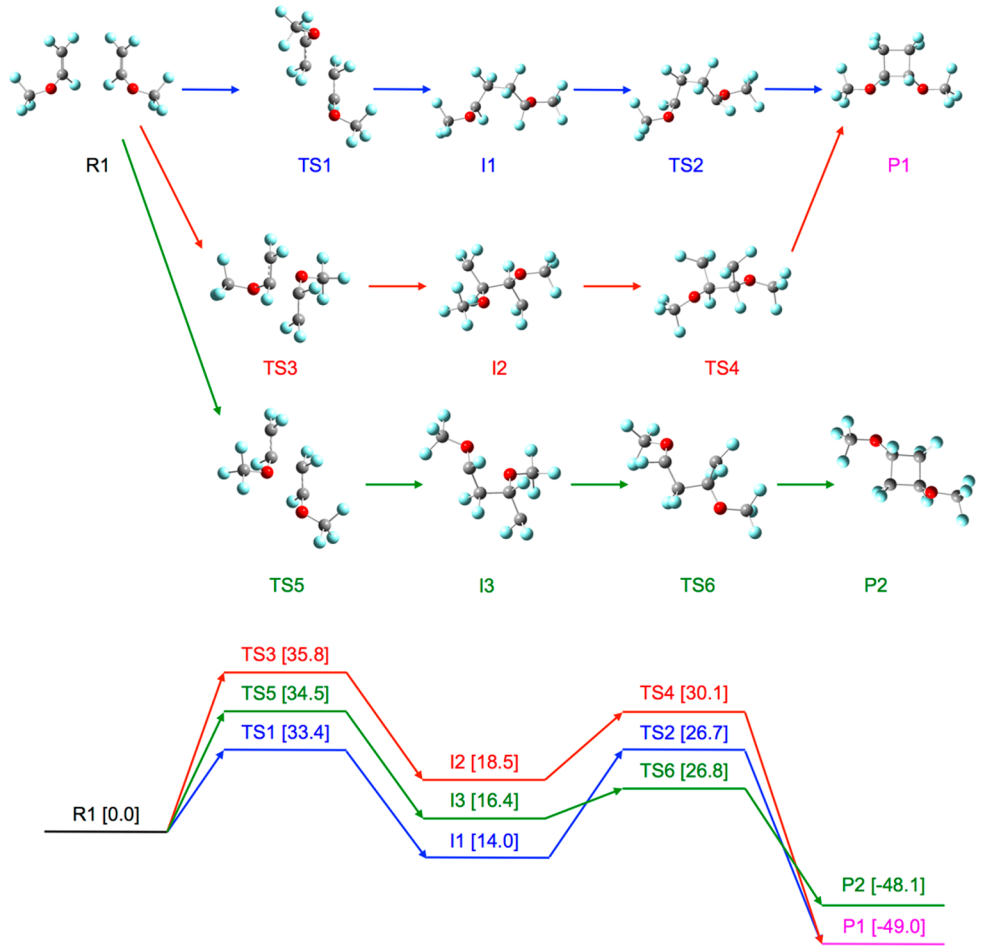


**Figure 6.** Full proposed reaction mechanisms for the three different routes of cycloaddition (head-to-head, head-to-tail, and tail-to-tail) for TFVE. The geometries are at the top, and a qualitative energy diagram (relative energies in kcal/mol) is at the bottom.

**Table 1. Geometric Parameters for the Cyclodimerization of Two TFVE Molecules**[a]

| | 1st TS | I | 2nd TS | P |
|---|---|---|---|---|
| C1−C3 | | | | |
| *d*(2−1−3−4) | 175.30 | 167.87 | 41.95 | 14.27 |
| *b*(1−3) | 1.75 | 1.55 | 1.54 | 1.56 |
| *b*(2−4) | | | 2.63 | 1.56 |
| C1−C4 | | | | |
| *d*(2−1−4−3) | −175.41 | −162.94 | 47.99 | −16.28 |
| *b*(1−4) | 1.75 | 1.56 | 1.54 | 1.55 |
| *b*(2−3) | | | 2.65 | 1.55 |
| C2−C3 | | | | |
| *d*(1−2−3−4) | −171.66 | 52.53 | 39.84 | −16.28 |
| *b*(2−3) | 1.80 | 1.55 | 1.54 | 1.55 |
| *b*(1−4) | | | 2.61 | 1.55 |

[a]Bond lengths are shown in angstroms, and dihedral angles are shown in degrees.

The theoretical results align well with the experimental results, which supports our proposed reaction pathway. Given the proposed reaction pathway it is now possible to compare these computations to previous experimental findings with small molecules in an effort to improve conditions for TFVE-BP polymerization.

**3.5. Molecular Weight and Reaction Conditions from Literature.** One of the drawbacks of TFVE polymer chemistry is the difficulty in producing high molecular weight materials. This can be remedied through use of a catalyst,[29] but that reduces one of main benefits of this chemistry for commercial applications. If the molecules need to twist throughout the course of the reaction pathway, then it is conceivable that a polymerization with this chemistry will have a viscosity-dependent rate. As the polymerization proceeds, polymer chains entangle, increasing the viscosity. This study suggests that this increase in viscosity could inhibit the reaction rate. To probe this theory, literature was reviewed in an attempt to find evidence to support this hypothesis. All reactions listed in Table 3 are the polymerization of 4,4′-bis(4-trifluorovinyloxy)-biphenyl (TFVE-BP) (CAS = 134130-19-1) under various conditions. These conditions include solvent-free or bulk polymerizations and use of diphenyl ether (DPE) and perfluorotetradecahydrophenanthrene (PFTDP) solvents.

Since this polymerization follows second-order, step-growth kinetics, the molecular weight ($M_w$) will increase linearly with time (see the derivation in the SI). Assuming that the activation energy is 25 kcal/mol for this condensed-phase polymerization,[34] the equivalent reaction time at 118 °C can be calculated for each of the reaction conditions found in the literature. Plotting molecular weight vs this effective time at 118 °C produces a linear trend for bulk polymerizations ($R^2$ = 0.942) where addition of solvent produces high molecular weight material more rapidly; see Figure 9. Although the concentration of reactive species is lower when solvent is



DOI: 10.1021/acs.joc.7b00597
J. Org. Chem. 2017, 82, 6578−6585

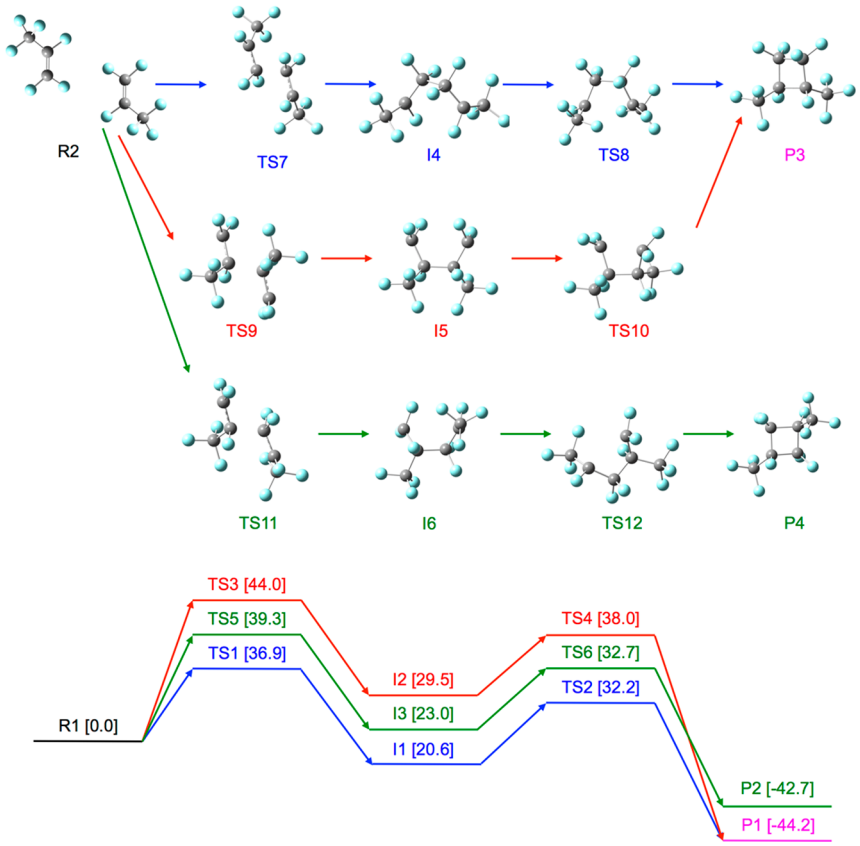


**Figure 7.** Full proposed reaction mechanisms for the three different routes of cycloaddition (head-to-head, head-to-tail, and tail-to-tail) for HFP. The geometries are at the top, and a qualitative energy diagram (relative energies in kcal/mol) is at the bottom.

**Table 2. Geometric Parameters for the Cyclodimerization of Two HFP Molecules**[a]

| | 1st TS | I | 2nd TS | P |
|---|---|---|---|---|
| C1−C3 | | | | |
| *d*(2−1−3−4) | 171.58 | 69.01 | 40.84 | 11.28 |
| *b*(1−3) | 1.75 | 1.55 | 1.54 | 1.56 |
| *b*(2−4) | | | 2.59 | 1.56 |
| C1−C4 | | | | |
| *d*(2−1−4−3) | −172.34 | −15.14 | 33.27 | 10.80 |
| *b*(1−4) | 1.79 | 1.58 | 1.55 | 1.56 |
| *b*(2−3) | | | 2.54 | 1.55 |
| C2−C3 | | | | |
| *d*(1−2−3−4) | 172.05 | 58.40 | 36.98 | 10.84 |
| *b*(2−3) | 1.75 | 1.55 | 1.54 | 1.55 |
| *b*(1−4) | | | 2.62 | 1.56 |

[a]Bond lengths are shown in angstroms, and dihedral angles are shown in degrees.

added, the rate of the reaction is accelerated. This coincides with our hypothesis that higher viscosity may inhibit rotation and limit the rate of reaction.

An additional way for producing high molecular weight materials may be to go to higher temperatures. As polymers heat up, the viscosity decreases. There is a general trend in molecular weight produced and reaction temperature; see Figure 10. This trend looks similar to the behavior of viscosity vs temperature for a similar polymer found in literature.[4]

As higher molecular weights are desired, two methods of achieving this without catalyst are proposed; both involve reducing the viscosity of the reaction. First, using a solvent or

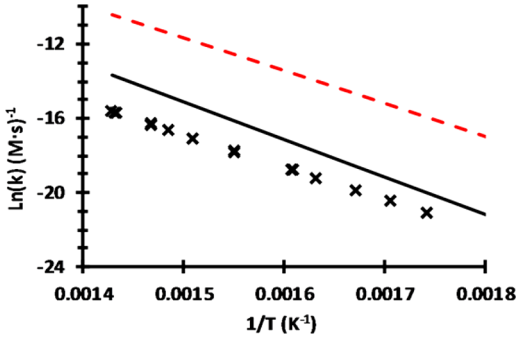


**Figure 8.** Rates of reactions in the temperature range of 127−393 °C show good agreement between experiment (X) and simulated kinetic data for HFP (black solid line) and TFVE (red dotted line).

**Table 3. List of Reactions and Conditions for the Polymerization of TFVE-BP (wt % Monomer)**

| *T* (°C) | time (h) | solvent | $M_w$ | PDI | ref |
|---|---|---|---|---|---|
| 250 | 108 | bulk | 219081 | 6.65 | 30 |
| 220 | 3 | PFTDP (28 wt %) | 103300 | 2.55 | 31 |
| 220 | 3 | PFTDP (28 wt %) | 116400 | 1.89 | 31 |
| 215 | 3 | PFTDP (28 wt %) | 89719 | 3.05 | 4 |
| 200 | 72 | bulk | 58000 | N/A | 29 |
| 200 | 4 | DPE (38 wt %) | 7500 | 1.31 | 32 |
| 180 | 48 | bulk | 40000 | N/A | 29 |
| 160 | 12 | bulk | 7300 | N/A | 33 |
| 160 | 16 | bulk | 14700 | N/A | 29 |



DOI: 10.1021/acs.joc.7b00597
J. Org. Chem. 2017, 82, 6578−6585

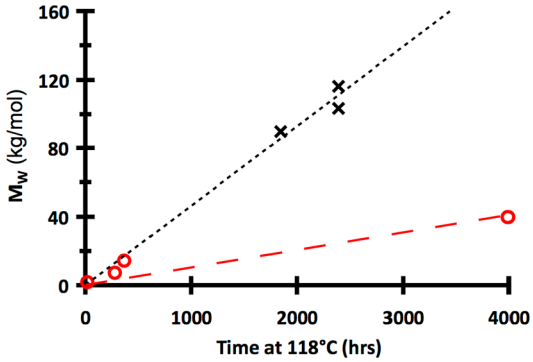


**Figure 9.** Plot of molecular weight vs reaction time at 118 °C showing linear trend between molecular weight and effective reaction time for the reaction with solvent (X) and without (O).

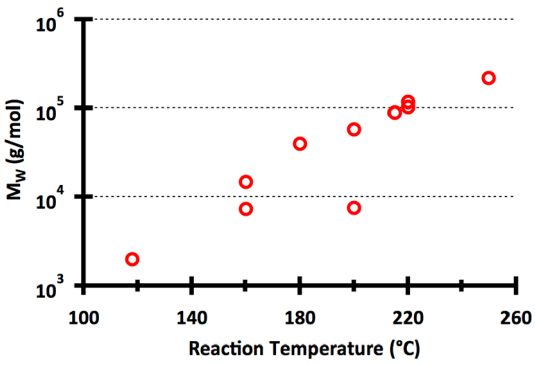


**Figure 10.** Temperature vs molecular weight for the polymerization of TFVE-BP.

plasticizer at 220 °C will product high molecular weight material in several hours. A second method is to use high temperature in excess of 240 °C and a bulk (solvent free) polymerization. To provide further support for the proposed reaction mechanism, we encourage a study tracking molecular weight and viscosity vs time for a bulk polymerization and polymerization using PFTDP (28 wt %). Using a temperature of 200 °C and time of 96 h would be preferred.

## 4. CONCLUSIONS

Gas-phase calculations were performed on TFVE and HFP dimerizations, resulting in evidence for a reaction mechanism involving two SCO-TSs. Previously a diradical intermediate was observed using EPR, but this study provides insight into how this reaction may take place. Utilizing a Newton−Raphson minimization algorithm, 12 SCO-TSs were found for the two reactions studied, the result of 3 pathways for each reaction, each involving two SCO-TSs. The activation energy for head-to-head addition was the lowest in both cases, indicating this is the most probable pathway found. Additionally, the main product observed experimentally (1,2 adduct) was the product of this pathway. The calculated reaction kinetics was in excellent agreement with previously reported experiments. Based on the computed results, higher temperatures and lower viscosities are advised to keep cycloaddition polymerizations catalyst free. This will enable the rotation of polymer chains and avoid slowing reaction rates, theoretically allowing for higher molecular weights produced more rapidly.

## ■ ASSOCIATED CONTENT

### Supporting Information

The Supporting Information is available free of charge on the ACS Publications website at DOI: 10.1021/acs.joc.7b00597.

Energy for all stationary points, relative reaction rates for different pathways, coordinates of all spin crossover transition states ($E_m$ = 1 = $E_m$ = 3), and derivation of molecular weight vs time for condensation polymerizations (PDF)

## ■ AUTHOR INFORMATION


### Corresponding Authors

*E-mail: svyas@mines.edu. Tel: 303-273-3632.
*E-mail: cmmaupin@mines.edu. Tel: 303-273-3197.

### ORCID

Andrew M. Herring: 0000-0001-7318-5999
Shubham Vyas: 0000-0002-5849-8919
C. Mark Maupin: 0000-0001-8593-7035


### Notes

The authors declare no competing financial interest.

## ■ ACKNOWLEDGMENTS

We thank DOE EERE Grant No. DE-EE0006363 for support and funding for this research. Additionally, the computational resources for this work were provided by the Colorado School of Mines Campus Computing, Communications, and Information Technologies.

## ■ REFERENCES


(1) Lewis, E. E.; Naylor, M. A. *J. Am. Chem. Soc.* **1947**, *69*, 1968−1970.
(2) Bartlett, P. D.; Montgomery, L. K.; Seidel, B. *J. Am. Chem. Soc.* **1964**, *86*, 616−622.
(3) Montgomery, L. K.; Schueller, K.; Bartlett, P. D. *J. Am. Chem. Soc.* **1964**, *86*, 622−628.
(4) Babb, D. A.; Ezzell, B. R.; Clement, K. S.; Richey, W. F.; Kennedy, A. P. *J. Polym. Sci., Part A: Polym. Chem.* **1993**, *31*, 3465−3477.
(5) Smith, D. W., Jr.; Babb, D. A. *Macromolecules* **1996**, *29*, 852−860.
(6) Mifsud, N.; Mellon, V.; Jin, J.; Topping, C. M.; Echegoyen, L.; Smith, D. W. *Polym. Int.* **2007**, *56*, 1142−1146.
(7) Spraul, B. K.; Suresh, S.; Jin, J.; Smith, D. W., Jr. *J. Am. Chem. Soc.* **2006**, *128*, 7055−7064.
(8) Smith, D. W.; Chen, S.; Kumar, S. M.; Ballato, J.; Topping, C.; Shah, H. V.; Foulger, S. H. *Adv. Mater.* **2002**, *14*, 1585−1589.
(9) Qian, G.; Smith, D. W.; Benicewicz, B. C. *Polymer* **2009**, *50*, 3911−3916.
(10) Ford, L. A.; DesMarteau, D. D.; Smith, D. W. *J. Fluorine Chem.* **2005**, *126*, 651−658.
(11) Jin, J. Y.; Smith, D. W.; Topping, C. M.; Suresh, S.; Chen, S. R.; Foulger, S. H.; Rice, N.; Nebo, J.; Mojazza, B. H. *Macromolecules* **2003**, *36*, 9000−9004.
(12) Klukovich, H. M.; Kean, Z. S.; Iacono, S. T.; Craig, S. L. *J. Am. Chem. Soc.* **2011**, *133*, 17882−17888.
(13) Harvey, J. N. *Wiley Interdisciplinary Reviews: Computational Molecular Science* **2014**, *4*, 1−14.
(14) Zhao, Y.; Truhlar, D. G. *Theor. Chem. Acc.* **2008**, *120*, 215−241.
(15) Ditchfield, R. *J. Chem. Phys.* **1971**, *54*, 724−728.
(16) Frisch, M. J.; Trucks, G. W.; Schlegel, H. B.; Scuseria, G. E.; Robb, M. A.; Cheeseman, J. R.; Scalmani, G.; Barone, A. V.; Mennucci, B.; Petersson, G. A.; Nakatsuji, H.; Caricato, M.; Li, X.; Hratchian, H. P.; Izmaylov, A. F.; Bloino, J.; Zheng, G.; Sonnenberg, J. L.; Hada, M.; Ehara, M.; Toyota, K.; Fukuda, R.; Hasegawa, J.; Ishida, M.; Nakajima, T.; Honda, Y.; Kitao, O.; Nakai, H.; Vreven, T.; Montgomery, J. A., Jr.;




DOI: 10.1021/acs.joc.7b00597
*J. Org. Chem.* 2017, 82, 6578−6585

Peralta, J. E.; Ogliaro, F. o.; Bearpark, M. J.; Heyd, J.; Brothers, E. N.; Kudin, K. N.; Staroverov, V. N.; Kobayashi, R.; Normand, J.; Raghavachari, K.; Rendell, A. P.; Burant, J. C.; Iyengar, S. S.; Tomasi, J.; Cossi, M.; Rega, N.; Millam, N. J.; Klene, M.; Knox, J. E.; Cross, J. B.; Bakken, V.; Adamo, C.; Jaramillo, J.; Gomperts, R.; Stratmann, R. E.; Yazyev, O.; Austin, A. J.; Cammi, R.; Pomelli, C.; Ochterski, J. W.; Martin, R. L.; Morokuma, K.; Zakrzewski, V. G.; Voth, G. A.; Salvador, P.; Dannenberg, J. J.; Dapprich, S.; Daniels, A. D.; Farkas, Ã. d. n.; Foresman, J. B.; Ortiz, J. V.; Cioslowski, J.; Fox, D. J. *Gaussian 09*; Gaussian, Inc.: Wallingford, CT, 2009.

(17) Clark Ligon, S.; Krawiec, M.; Kitaygorodskiy, A.; Smith, D. W. *J. Fluorine Chem.* **2003**, *123*, 139−146.

(18) Chachiyo, T.; Rodriguez, J. H. *J. Chem. Phys.* **2005**, *123*, 94711−94719.

(19) Rudolf, K.; Bock, W. K. *The Data Analysis BriefBook (Accelerator Physics)*; Springer, 1998.

(20) Landau, L. *Phys. Z. Sowjetunion* **1932**, *2*, 46−51.

(21) Zener, C. In *Proceedings of the Royal Society of London A: Mathematical, Physical and Engineering Sciences*; The Royal Society: 1932; Vol. *137*, pp 696−700.

(22) Glowacki, D. R.; Liang, C. H.; Morley, C.; Pilling, M. J.; Robertson, S. H. *J. Phys. Chem. A* **2012**, *116*, 9545−9560.

(23) Gannon, K. L.; Blitz, M. A.; Liang, C.-H.; Pilling, M. J.; Seakins, P. W.; Glowacki, D. R.; Harvey, J. N. *Faraday Discuss.* **2010**, *147*, 173−178.

(24) Plane, J. M.; Whalley, C. L.; Frances-Soriano, L.; Goddard, A.; Harvey, J. N.; Glowacki, D. R.; Viggiano, A. A. *J. Chem. Phys.* **2012**, *137*, No. 014310.

(25) Chambers, R. D. In *Fluorine in Organic Chemistry*; Blackwell Publishing Ltd.: Oxford, UK, 2004.

(26) Clark Ligon, S.; Krawiec, M.; Kitaygorodskiy, A.; Smith, D. W. *J. Fluorine Chem.* **2003**, *123*, 139−146.

(27) Wlassics, I. *J. Fluorine Chem.* **2004**, *125*, 1519−1528.

(28) Atkinson, B.; Tsiamis, C. *Int. J. Chem. Kinet.* **1979**, *11*, 1029−1043.

(29) Shane, S.; Mao, A. R. S. *3M Innovative Properties Company*. US6,646,075B2, 2003.

(30) Kalaw, G. J. D.; Wahome, J. A. N.; Zhu, Y.; Balkus, K. J.; Musselman, I. H.; Yang, D.-J.; Ferraris, J. P. *J. Membr. Sci.* **2013**, *431*, 86−95.

(31) Babb, D. A. *Fluoropolymers 1: Synthesis* **2002**, 25.

(32) Huang, X.; Lu, G.; Peng, D.; Zhang, S.; Qing, F. -l. *Macromolecules* **2005**, *38*, 7299−7305.

(33) Park, J.; Oh, J. M.; Creager, S. E.; Smith, D. W., Jr. *Chem. Commun. (Cambridge, U. K.)* **2012**, *48*, 8225−8227.

(34) Cheatham, C. M.; Lee, S.-N.; Laane, J.; Babb, D. A.; Smith, D. W., Jr. *Polym. Int.* **1998**, *46*, 320−324.



DOI: 10.1021/acs.joc.7b00597
*J. Org. Chem.* 2017, 82, 6578−6585